Cornflake Production Process: State Diagram and Water Mobility Characteristics

Abel E. Farroni & María del Pilar Buera

Food and Bioprocess Technology
An International Journal

ISSN 1935-5130

Food Bioprocess Technol
DOI 10.1007/s11947-014-1270-5

Springer

Food Bioprocess Technol
DOI 10.1007/s11947-014-1270-5

ORIGINAL PAPER

Cornflake Production Process: State Diagram and Water Mobility Characteristics

Abel E. Farroni · María del Pilar Buera

Received: 5 October 2013 / Accepted: 17 January 2014

Abstract The aim of this work was to fully understand the physicochemical events involved in the development of the cornflake structure, taking into consideration the water sorption characteristics and state changes in the solid phase as a function of temperature and water content. Complementarily, time-resolved proton nuclear magnetic resonance (^{1}H-TD-NMR) was used to evaluate the dynamic aspects at different stages of the classical cornflake production process. Processing had the effect of reducing the water sorption capacity of the samples and of increasing the sorption energy. While the minimal water content necessary to detect starch gelatinization was lower than the water content at which frozen water was detected by DSC (W=24%), water excess for an adequate cooking needs to be higher than this value. By describing the process using supplemented state diagrams, it was possible to delimitate regions in which the main components (starch and proteins) underwent specific changes such as gelatinization or crosslinking. The data of comparative mobility of water populations helped to understand the occurrence of those changes. The physical state of the samples could be established for each process stage, the matrix was soft and malleable when important internal and external forces were applied which allowed the change of shape, microstructure, and appearance of the product. Physical hardening occurred after toasting to create the typical expected crispy texture. The data of comparative mobility of proton populations helped to understand the occurrence of those changes, the conditions prevailing in each stage, and the physical state of the sample.

Keywords State diagrams · NMR · DSC · Water sorption isotherm · Molecular mobility · Cornflakes

A. E. Farroni (✉)
Laboratorio de Calidad de Alimentos, Suelos y Aguas,
INTA Pergamino, Av. Frondizi (Ruta 32) Km 4.5,
CC 31-B2700WAA, Pergamino, Buenos Aires, Argentina
e-mail: farroni.abel@inta.gob.ar

M. del Pilar Buera
Departamento de Industrias, Facultad de Ciencias Exactas y Naturales, Universidad de Buenos Aires, Intendente Güiraldes 100, C1428EGA, Ciudad de Buenos Aires, Argentina
e-mail: pilar@di.fcen.uba.ar

Introduction

Carbohydrates and proteins in food systems show water-sensitive phase transitions (e.g., melting, crystallization, protein denaturation, starch gelatinization) and state transitions (Roos 2003). Most of these transitions that occur at nonequilibrium conditions affect the materials' behavior at the processing stages and storage conditions of food systems (Rahman 2006). Supplemented temperature/composition state diagrams have demonstrated to be helpful in determining the feasibility of the occurrence of phase/state transitions (Slade et al. 1989; Levine and Slade 1992). These diagrams include the equilibrium curves and the nonequilibrium glass transition (T_g) curve, which allows establishing relationships with the time coordinate and, thus, with the dynamic behavior of the systems, providing that the thermal history of the samples is known.

A state diagram of a food system can be generated on the basis of composition (main soluble components, insoluble biopolymers, and water content) and of the critical points of their typical thermal or mechanical transitions. Then, the occurrence or not of some phenomena and their kinetics can be predicted by the relative position of the curves in the supplemented state diagram and of the experimental conditions at which the systems will be exposed (Buera et al. 2011a). Thus, supplemented state diagrams are increasingly used to describe food systems and processes (Madeka and Kokini 1996; Toufeili et al. 2002; Cuq et al. 2003; Sablani et al. 2009).

Published online: 04 February 2014

The study of molecular mobility has also been helpful for a better understanding of interactions at the molecular level in relation to different processes in food systems (Chinachoti et al. 2008). Nuclear magnetic resonance is a powerful technique to provide information on molecular dynamics of different components in complex systems (Farhat et al. 1996; Lin et al. 2006; Fundo et al. 2014). Low resolution proton nuclear magnetic resonance (^{1}H NMR) has been extensively used to study water mobility in food products (Chen et al. 1997; Tang and Hills 2001; Choi and Kerr 2003; Wang et al. 2004; Assifaoui et al. 2006; Curti et al. 2011).

Most of low moisture food products exist in disordered nonequilibrium amorphous state. The formation of amorphous structures during processing is particularly important for the stability of systems with long-term shelf-life requirements, such as frozen and low-water foods (Slade and Levine 1995; Roos et al. 1996). Breakfast cereals, increasingly consumed by adults and children, are among this type of foods. Cornflakes are produced either by flaking or extrusion techniques. In Argentina, flint corn varieties are suitable for using in the traditional gelatinization flaking process (Fast 2000). Briefly, this process starts with the milling of corn kernels for obtaining endosperm chunks called grits. Corn grits are steam-batch cooked in the presence of water and sugar, salt, or malt extract. The cooked grits are partially dried by a hot air current and are then allowed to rest in a bin for several hours to allow moisture homogenization, this process is called tempering. The flaking process is performed by compressing cooked grits between two steel rolls. The final toasting step is carried out under a hot-air current at approximately 200ºC. Along this process, samples undergo important chemical and physical changes. Gelatinization, flaking, and toasting processes imply physical transformations at microstructural and macroscopic levels. The approaches to controlling the structure and texture of cereal products have been mainly focused on semiempirical optimizations or on the selection of raw materials adapted to the process.

The aim of this work was to fully understand the physicochemical events involved in the development of the cornflake's structure, taking into consideration phase and state changes as a function of temperature and water content. Complementarily, proton mobility was analyzed in the main stages of processing.

Materials and Methods

Samples

Samples of four selected industrial process stages were provided by a local breakfast cereal manufacturer. Samples analyzed were raw grits (G), cooked grits (CG), tempered cooked grits (CG_t), flaked grits (FG), and corn flakes (CF). In order to obtain samples with different water content, they were equilibrated over saturated salt solutions at relative vapor pressures in the range of water activities (a_w) between 0.11 and 0.80 (LiCl 0.11, $MgCl_2$ 0.33, K_2CO_3 0.44, NaCl 0.75, KCl 0.84) (Greenspan 1977). For higher water contents, samples were sprayed with water and allowed to equilibrate overnight in sealed vessels. None of the analyzed samples presented any evidence of fungal growth during storage upon examination by ocular stereoscope (Unitron MS, NY, USA).

Water Content and Water Activity

After equilibration at controlled atmospheres, the a_ws of the systems were measured using an electronic dew-point water activity meter (Aqualab Series 3, Decagon Devices, Pullman, WA, USA). The water content of the systems was determined gravimetrically by difference in mass before and after drying of the samples in an oven at 105ºC to constant weight (AACC 1996 approved method 44–16), and the results were expressed in percent (%) mass fraction of water (W).

Water adsorption data were fitted to the Guggenheim-Anderson-de Boer (GAB) equation, which is the most widely employed model in food systems since it applies over a wide range of a_w (Lomauro et al. 1985; Samapundo et al. 2007; Yanniotis and Blahovec 2009). The GAB constants m_o, C, and k were obtained by transforming the GAB equation to the quadratic form:

$$\frac{a_w}{m} = \frac{k}{m_o}\left(\frac{1}{C-1}\right)a_w^2 + \left(\frac{C-2}{m_o C}\right)a_w + \frac{1}{m_o Ck} \quad (1)$$

where m is the equilibrium water content expressed in dry basis, a_w is the water activity, m_o is the GAB hydration limit water content, C is the Guggenheim constant that is related to the heat of sorption of the first layer on primary sites, and k is a factor correcting the properties of the water molecules sorbed after the primary sites were occupied in relation to the bulk liquid. The mean relative percent deviation of predicted water content values (%E) defined by Lomauro et al. (1985) was used as a criterion of fitness.

Water sorption surface area (S_w) was calculated from m_o by using Eq. 2 (Gregg and Sing 1982):

$$Sw = \frac{m_o Na}{M} \quad (2)$$

where S_w is expressed in $m^2 \cdot g^{-1}$, m_o is the GAB hydration limit water content, N is the Avogadro number ($6.02 \cdot 10^{23}$ molecules$\cdot$ mol^{-1}), a is the area occupied by a single water molecule ($10.6 \cdot 10^{-20}$ m^2), and M is the molar mass of water (18 $g \cdot mol^{-1}$).

Thermal Transitions

Approximately 15 mg of ground samples were weighed with a precision of ±0.01 mg, sealed into aluminum pans (40 μL

capacity), and loaded into a differential scanning calorimeter (DSC) (Mettler Toledo, model 822, Schwerzenbach, Switzerland). Heat flux was measured with a resolution better than 0.04 μW. All experiments were performed in duplicate following the same protocol. The instrument was calibrated using indium, zinc, and lead. An empty pan was used as reference. The DSC thermograms were obtained from −50 ºC to 150 ºC at a heating rate of 10 ºC·min^{-1}. This heating rate is commonly selected in order to observe biopolymer transitions clearly (Gabbott 2008). All thermograms were analyzed using STAR^e Software v. 6.1 (Mettler Toledo, Schwerzenbach, Switzerland). The glass transition temperature (T_g) was determined as the onset temperature of the discontinuities in heat flow versus temperature curves (indicating a change in specific heat). Onset temperature and enthalpy of gelatinization were obtained, integrating the area under the transition curve.

In order to model the effect of water on the glass transition temperature of samples, the data obtained for grits and cornflakes were fitted to the Gordon and Taylor equation (G-T) (Gordon and Taylor 1952), Eq. 3.

$$T_g = \frac{W_1 T_{g1} + k W_2 T_{g2}}{W_1 + k W_2} \tag{3}$$

where T_{g1} and T_{g2} are the onset temperatures of the glass transitions of the total amorphous solids and of pure water, respectively, W is the mass fraction of each component, and k is a constant which characterizes the effect of the second component (water, in this case) on the T_g values. If the ratio T_{g1}/T_{g2} is high (the T_g value of the first pure component is much higher that that of the second component), k is also high, and the second component will have a higher effect on the T_g value of the mixture (Katkov and Levine 2004).

Time-Resolved Proton Nuclear Magnetic Resonance (^{1}H-TD-NMR)

Time-resolved proton nuclear magnetic resonance (^{1}H-TD-NMR) was used to evaluate the molecular mobility of solids and water, measuring the spin-spin relaxation constants (T_2). A low resolution time-resolved RMN equipment (Bruker Minispec, model mq20, Bruker Biospin GmbH, Rheinstetten, Germany) operating with a 0.47 T magnetic field, 20 MHz frequency, and 40 ºC magnet temperature was used. Milled samples were inserted in 10-mm diameter glass tubes for analysis. The relaxation times were measured with three different pulse sequences, according to the water content of the samples. Free induction decay (FID) analysis was measured after a 90º pulse. FID signal is affected by inhomogeneities of the magnetic field: nuclei in one part of the sample experience and a magnetic field slightly different from that experienced by identical nuclei in another region. The T_2 measured in these conditions is called apparent T_2. However, in solid samples, when the relaxation times are in the order of microseconds, the apparent T_2 are very close to the intrinsic T_2, as reported previously by Fullerton and Cameron (1988). The second pulse sequence employed was the Hahn spin echo (90º-τ-180º) (Hahn 1950; Ruan and Chen 1998) with an interpulse time (τ) range from 0.001 to 4 ms. It was appropriate to register the full signal decay for intermediate T_2 values (covering the range between microseconds and milliseconds). Finally, the Car-Purcell-Meiboom-Gill (CPMG) pulse sequence was applied, which consists of a 90º pulse followed by a series of 180º pulses at time τ, 3τ, 5τ etc., obtaining echoes at times 2τ, 4τ, 6τ etc. This sequence was suitable for measuring relaxation times of 0.5 ms and above (Ruan and Chen 1998).

The decay envelopes were fitted to monoexponential (Eq. 4) or biexponential (Eq. 5) equations according to best fitting results.

$$I = A e^{-t/T_2} \tag{4}$$

where I represents the NMR signal intensity at time t, T_2 is the relaxation time constant, and A is proportional to the number of protons generating the signal.

$$I = A_1 e^{\left(-t/T_{2S}\right)} + A_2 e^{\left(-t/T_{2L}\right)} \tag{5}$$

where I represents the NMR signal intensity at time t, as in Eq. 4. The relaxation time constant T_{2S} corresponds to the less mobile proton fraction. A_1 is proportional to the number of these protons. The relaxation time constant T_{2L} corresponds to protons with higher mobility, as compared to those with relaxation time constant T_{2S}, and A_2 is proportional to the number of these protons.

All determinations were performed in duplicate, and results were averaged. Curve fitting and graphical analysis was performed using GraphPad Prism version 5.00 for Windows (GraphPad Software, San Diego, CA, USA).

Results and Discussion

Water Activity, Water Sorption, and Glass Transition Temperature

The a_w for the systems at the different stages were as follows: 0.68 for the raw grits, 0.95 at the end of cooking; 0.88 after drying and tempering; 0.83 after flaking and 0.20 after toasting. The low a_w value for the final product is important to microbiological stability and shelf life. Table 1 shows the best-fit parameters for the GAB equation fitted to the water sorption data. Determination coefficients (R^2) were between 0.988 and 0.996, and %E for water content were 5.2 % and lower indicating the good predictive values of the GAB

Table 1 Best-fit parameters of GAB equation fitted to sorption isotherm data for the different cornflake processing stages

Parameter	G	CGt	FG	CF
m_o (%)	9.1 (1)	5.7 (0.4)	6.4 (0.4)	5.8 (0.4)
S_w ($m^2\ g^{-1}$)	355 (35)	213 (14)	241 (14)	220 (21)
k	0.66 (0.03)	0.89 (0.01)	0.83 (0.02)	0.90 (0.01)
C	7.5 (1.3)	21 (16)	13 (6)	2.9 (0.5)
R^2	0.9880	0.9904	0.9894	0.9959
%E	3.4	4.8	4.2	5.2

Standard error values between brackets

G raw grit, *GCt* tempered cooked grit, *FG* flaked grit, *CF* cornflakes

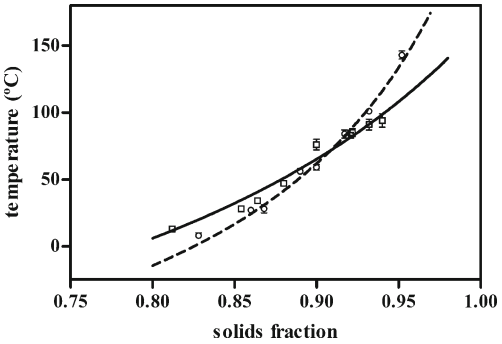

Fig. 1 Glass transition temperature of raw grits (□) and cornflakes (○) modeled as function of solid mass fraction (*bars* on symbols represent standard deviation). Best-fit parameter for Gordon and Taylor equation for grits were as follows: T_{g1} 166±9ºC, k 4.5±0.4, and R^2 0.974; and for cornflakes, T_{g1} 265±12ºC, k 9.3±0.6, and R^2 0.990

equation when applied to these data. The value for hydration limit (m_o) was higher for raw grit (9.1 %) than for processed samples which showed values from 5.7 to 6.4 %. This reduction in the water sorption of primary sorption sites is better reflected in the value of S_w which also decreased by processing. The parameter C is the sorption energy constant, related to the difference of free enthalpy (standard chemical potential) of the sorbate molecules in the pure liquid state and in the first sorbed state. *C*-obtained values increased in the cooking and flaking stages, but after the toasting stage, the lowest C value was obtained. The additional constant of the GAB model sorption k accounts for the fact that the state of the sorbate molecules in the layers beyond the first one is the same, but different to the pure liquid state. The *k*-obtained values were close to, but less than one as has been reported for food samples (Palou et al. 1997; Samapundo et al. 2007; Cova et al. 2010), being raw grits of the samples with the lowest k value (0.663).

The global interpretation of the water sorption parameters indicated that processing had the effect of reducing the water sorption capacity of the samples and of increasing the sorption energy up to the last toasting step. Particularly, CF sorption isotherm showed less sigmoid shape and had lower water contents as compared to the rest of the samples at the same a_w. GAB parameters for raw grits are in agreement with those reported by Timmermann et al. (2001) and Samapundo et al. (2007) for corn flour.

The different states of water have been related to water sorption models, and in the last decades, concepts widely used as "bound water," "monolayer water," and "free water" were questioned (Levine and Slade 1989, 1991). The use of terms related to the experimental observations seems more appropriate, i.e., hydration limit and frozen water (Buera et al. 2011b).

Figure 1 shows the glass transition temperature for corn flakes and raw grits as a function of water content expressed as solid fraction. As described for several biopolymers and for cornflakes in previous works (Thiewes and Steeneken 1997; Chung and Lim 2004; Farroni et al. 2008), an endothermic transition was found at about 50 °C on DSC thermograms of the different samples. As this event disappeared in an immediate rescan, when the T_g values were close to 50 °C, and therefore overlapped with the endothermic event, they could be measured in a second DSC run. Glass transition onset temperatures were modeled as a function of water content using Gordon and Taylor (G-T) equation (Eq. 3). The G-T equation was originally developed for binary systems, but its use has been extended to complex systems considering the mix of solids as a whole (component 1) and water as the second component (Chen and Yeh 2001; Cuq et al. 2003; Sandoval et al. 2009). Taking this late approach, the obtained correlation coefficients for the studied samples were 0.974 for G and 0.990 for CF (shown in Fig. 1) indicating that experimental values were in good agreement with the G-T model.

Frozen Water

As W value increased, water reached enough mobility, and it could crystallize when cooling to −70 °C. The proportion of water that could freeze is frequently named as "free" water in an attempt to differentiate it from water with mobility restricted by interactions with solids. As discussed earlier, this name could lead to misinterpretations of the states of water in a complex matrix as foods. The presence of frozen water was observed on DSC experiments as endothermic events centered close to 0 ºC produced by the melting of ice crystals (Fig. 2).

The enthalpy of this endothermic peak is proportional to the amount of water that was frozen during the previous cooling. Figure 3 shows a plot of water-melting enthalpy (ΔH_m) as function of water content. The W value corresponding to the appearance of frozen water could be obtained by extrapolating the linear fit to ΔH_m=0. The result was 24±2 % for grits and 25±6 % for cornflakes. Using the same approach, Sablani et al. (2009) reported an unfreezable water content of 36.4 % for rice.

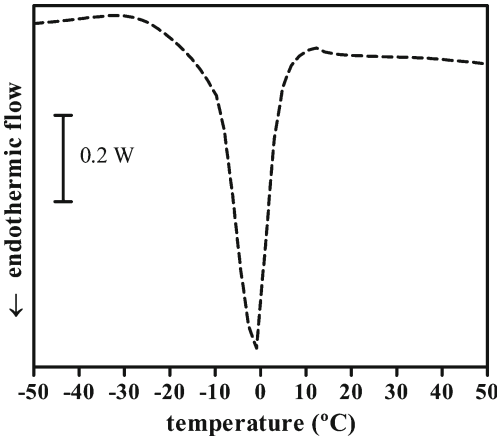

Fig. 2 DSC thermogram showing the endothermic melting peak of water in a cornflake sample containing 36.4 % water, previously frozen at −70 ºC and heated at 10 ºC·m^{-1}

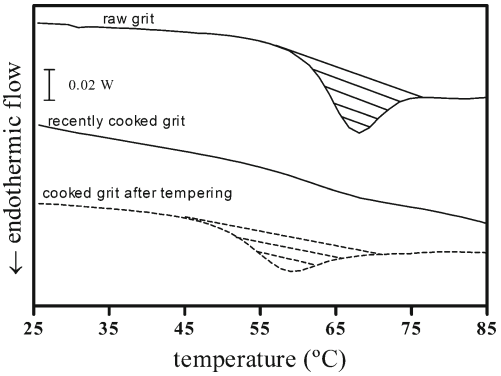

Fig. 4 DSC thermograms showing starch gelatinization endotherms in raw grits, which disappeared when measured immediately after cooking (*solid line*), and reappeared in tempered cooked grit (*dashed line*), due to the melting of the retrograded starch

Starch Gelatinization

In the cooking process, the starch was completely gelatinized as could be seen running a DSC experiment before and immediately after cooking. The endothermic peak corresponding to starch gelatinization disappeared after cooking. After tempering, starch underwent retrogradation, and the gelatinization of the retrograded starch could be seen in a DSC run. The corresponding endotherm was wider and started at a lower temperature than gelatinization of native starch (Fig. 4), also the enthalpy (ΔH) was lower indicating that the new generated crystalline structure, after retrogradation, was less ordered than the native one (Liu et al. 2007).

The onset temperature of starch gelatinization (T_{oG}) for raw grits was measured in samples at different water contents. The lowest W value at which a small endotherm, attributable to gelatinization, was detectable was 16 %. The T_{oG} for that first gelatinization was 113 ºC, and the enthalpy was considerably reduced as compared to the ΔH value corresponding to gelatinization in excess of water. It is interesting to note that the minimal water content necessary to detect starch gelatinization was lower than the water content at which frozen water was detected by DSC (W=24 %), indicating that only a small fraction of starch underwent thermal transition when water availability was restricted.

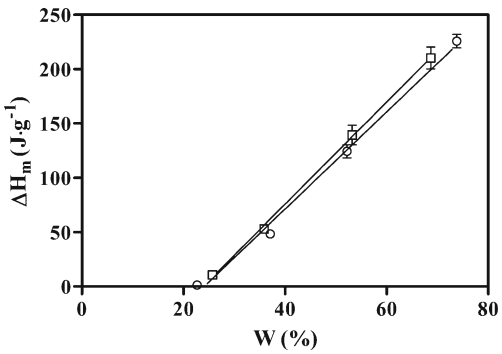

Fig. 3 Melting enthalpy of frozen water (ΔH_m) as a function of the mass fraction of water (W) for raw grits (□) and cornflakes (○). *Bars* on symbols represent standard deviation

As water content increased, the T_{oG} values decreased and the gelatinization enthalpy values increased, up to constant values with an average of 60.1 ºC were reached at water content higher than 40 %. At W values higher than 40 %, water was in a separated phase from starch, and in such excess that the addition of more water had no significant effect on the gelatinization temperature. At W values lower than 40 %, higher temperatures were needed in order to achieve the mobility necessary to melt starch crystals. Fast (2000) reported that proper cooking for corn flake production could be obtained using W values of at least 32 %. According to this, water excess for an adequate cooking needs to be higher than the minimum necessary to form a separate phase and freeze (W=24 %).

Nuclear Magnetic Resonance

Figure 5 shows the relaxation time constants of the different proton populations that were measured in cornflakes using ^{1}H-TD-NMR. Cornflakes with a wide range of water contents were selected as representative of the samples studied. Different ^{1}H NMR techniques were used with the aim of establishing the more appropriate pulse sequence and interpulse times, depending on the water content of the samples. A logarithmic time scale was used in order to show all the T_2 values, which differ in several magnitude orders from one sample to another. The graph was divided in three zones, according to the magnitude of the proton relaxation times, which are related to water mobility. At low water contents (zone I), only one proton population could be observed. This population (T_{2FID}) was characterized by a relaxation time near 8 μs, when determined using free induction decay (FID) analysis after a 90º pulse. It can be attributed to protons of solids and of water molecules closely interacting with them (Chen et al. 1997; Choi and Kerr 2003; Schmidt 2004).

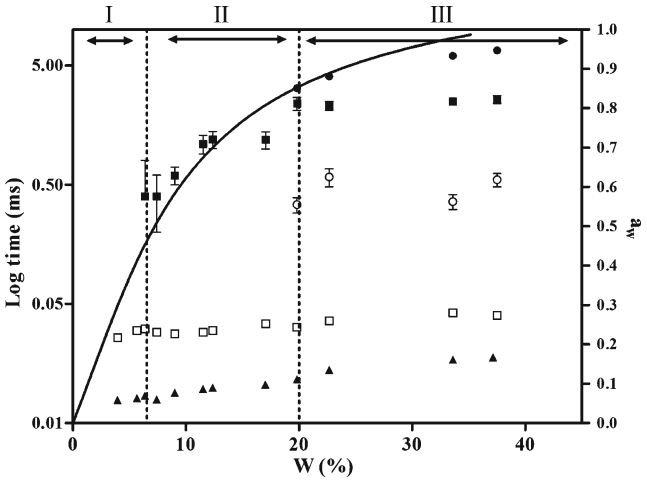

Fig. 5 Relaxation time constants and a_w values for the different proton populations of cornflakes, measured by ^{1}H-TD-NMR. T_{2FID} (▲), T_{2SHahn} (□), T_{2LHahn} (■), T_{2SCPMG} (○), T_{2LCPMG} (●), and GAB equation fitted to the water sorption isotherm (——). *Bars* on symbols represent 95 % confidence interval (when *bars* are not visible, they are hidden behind the symbol). Three zones related to water mobility are indicated at the top of the chart

Only the relaxation times of fast relaxing protons (which are in the microsecond range) can be correctly measured without a 180º refocus pulse (Colquhoun and Goodfellow 1994). Thus, when molecular mobility increased and proton relaxation times were close or above 30 μs, the Hahn spin echo sequence (90º-τ-180º) (Hahn 1950) was used, in which the 180º pulse has the purpose of refocusing the signal.

When the Hahn spin echo sequence was applied, only one proton population was observed at water contents below 6.4 %, and two proton populations were detected starting at water content 6.4 % and higher. One of them, having short relaxation times (close to 30 μs) labeled as T_{2SHahn}, corresponds to the protons of solids and water closely related to solids, and was also present in zone I. The population having longer relaxation times was labeled as T_{2LHahn} and corresponds to more mobile protons which include the water molecules with less interaction with the solid so called multilayer. The appearance of these second relaxation time constants delimited the end of zone I and the start of zone II. It is remarkable that the water content corresponding to this limit was very close to the m_o value obtained from GAB equation for cornflakes (5.8 %).

At water contents higher than 20 %, relaxation times were in the millisecond range, and the T_2 determined by the Hahn sequence (T_{2SHahn} and T_{2LHahn}) remained constant when water content increased. When relaxation times are in the millisecond range, diffusion effects make nuclei to move from one region to another in the magnetic field while measurement is in progress. Small inhomogeneities in the field make nuclei to sense different file intensities while moving, reducing the echo amplitude (Carr and Purcell 1954). Therefore, Hahn spin echo sequence was no longer adequate for its study and T_2 values were obtained using the CPMG sequence. Below the water content of 20 %, only one water population was distinguishable, while at water content above 20 %, two populations were detectable by the CPMG technique. This confirmed that W= 20 % is the lower limit for using the CPMG sequence given that below this water content, the two proton populations could not be separated. The second zone (II) lies between m_o, hydration limit, and 20 % water content. The relaxation time constant that characterized the population with shorter relaxation time (T_{2SCPMG}) remained constant and close to 0.50 ms in the W range from 20 to 37.5 %. This T_2 value was shorter than the one measured using the Hahn spin echo sequence (T_{2LHahn}), and this effect was attributed to the use of different refocus techniques. The relaxation time constant corresponding to the population with the longest relaxation time was labeled as T_{2LCPMG}. The T_{2LCPMG} values increased up to 6.7 ms as water content increased to 37.5 %. This third proton population was attributed to the more mobile or "free" water. Furthermore, as T_{2LHahn} remained constant while T_{2LCPMG} increased in the W range 20–37.5 %, it is confirmed that above W=20 %, Hahn sequence is no longer appropriate to measure T_2. It is to be noted that the occurrence of frozen water measured by DSC was at 25±6 % water content. In this way, at W=20 %, a third population was detected by CPMG, close, but below the water content at which water molecules acquire enough mobility to observe frozen water by DSC.

Table 2 shows the water content and the relaxation time constants for the proton populations of samples taken at the different cornflake production stages. Different zones, as defined before according to the number of proton populations were observed, and are also indicated with Roman numerals in the table, and the proton populations found were indicated as T_{2I}, T_{2II}, and T_{2III}. The pulse sequence after which the FID was analyzed is also indicated.

Zone I was defined by the m_o water content obtained from the GAB equation as upper limit, and this was coincident with the detection of only one proton population (T_{2I}) by NMR. As we noted earlier, this water population corresponded to the protons of solids and water with close interaction with solids and therefore showing restricted mobility. The only stage of cornflake production that was in this zone was cornflake (CF) (m_o=5.8 %) which had the lowest water content (2.9 %) due to the toasting step at a high temperature.

Zone II was characterized by the presence of two proton populations, T_{2I} and T_{2II}, the latter (longer times) corresponding to more mobile protons and water molecules more weakly interacting with solids as compared to T_{2I} (shorter times). Two stages of cornflake production had water contents with populations corresponding to this zone: raw grits (G) with W= 13 %, higher than m_o (9.1 %), and flaked grits (FG) with W= 17 % resulting from the loss of water of the tempered grit produced by the compression of the flaking rolls. It is to be noted that no frozen water was detected on FG by DSC.

Table 2 Relaxation time constants (T_2) for the proton populations found in the different process stages of cornflake production process

Process stage	*W*	Pulse sequence	T_{2I}	T_{2II}	T_{2III}	Zone
G	13.0 (0.5)	Hahn	0.0250 (0.0001)	1.10 (0.07)		II
CG	42.5 (0.6)	Hahn-CPMG	0.046 (0.003)	0.96 (0,07)	10.80 (0.05)	III
CGt	21.6 (0.5)	Hahn-CPMG	0.035 (0.001)	0.18 (0.04)	3.1 (0.06)	III
FG	17.5 (0.5)	Hahn	0.0340 (0.0007)	1.90 (0.07)		II
CF	2.9 (0.2)	One 90º pulse	0.0070 (0.0002)			I

Mean (in ms) and standard deviation in parentheses

G raw grit, *GC* cooked grit, *GCt* tempered cooked grit, *FG* flaked grit, *CF* cornflakes, T_{2I} short relaxation time population, T_{2II} medium relaxation time population, T_{2III} longer relaxation time population

When a third population with a higher mobility was detectable by NMR, it was considered the upper *W* limit of zone II and the beginning of zone III. According to the proton mobility, this occurred at 20 % water content. As we noted earlier, DSC confirmed the appearance of water with mobility enough to freeze quite easily at 25 % in raw grits and humidified cornflakes. Therefore, it is reasonable to assume that this limit for the appearance of frozen water, also called "free" water, is applicable for all the samples studied here. It is quite difficult to assign this limit from the water sorption isotherm itself (Timmermann and Chirife 1991); therefore, the combination of NMR and DSC techniques were used here for a better definition of the limit for the third state of water mobility than that provided by the water sorption isotherm analysis. Considering that NMR and DSC techniques are based on different concepts, the detection of the third water population by both techniques occurred at quite similar *W* values (20 % and 25 %, respectively).

The cooking stage occurred in the zone III, where the high molecular mobility is necessary to achieve the extensive water starch interaction that leads to a complete starch gelatinization at the temperature of cooking. In tempered cooked grits, three proton populations were also detected. After drying the tempered cooked grits, the water content was 21.6 %, close to the lower limit of zone II. The high water mobility in this stage was also important for browning and starch retrogradation as will be discussed later.

Integrated State Diagram

The T_g and T_{oG} as function of *W* curves were combined in order to assemble the state diagrams which are useful to analyze and understand the different phenomena taking place at each stage of cornflakes processing (Figs. 6 and 7). The reaction curve, as described by Madeka and Kokini (1996), corresponding to the zein crosslinking, which results in polymer thermosetting, is also shown. In Fig. 6 a, b, raw grit T_g curve was used as reference in order to indicate the limit of the glassy zone, and in Fig. 7, cornflake T_g curve was used. The water mobility zones, according to the different water content as measured by NMR, were indicated below the *x* axis. The amount of different proton populations present in the NMR experiment at 40 °C was indicated for each zone.

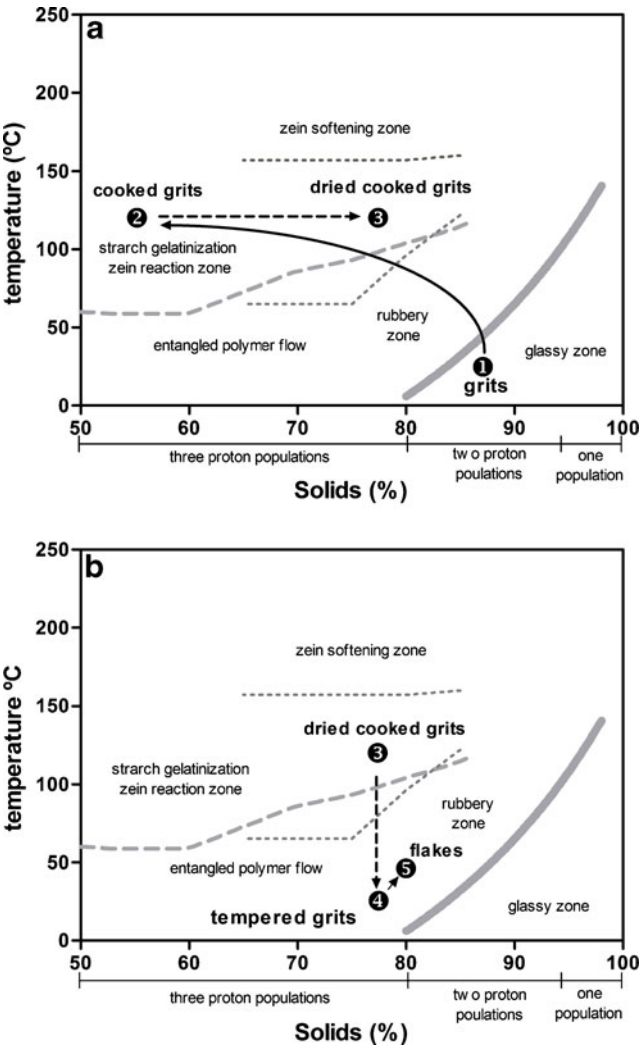

Fig. 6 State diagram for classical cornflake production process. **a** Cooking and drying stages. **b** Tempering and flaking stages. Solid line represents *Tg* curve for raw grits, dashed line represents starch gelatinization onset temperature, and dotted line represents onset temperatures of zein crosslinking reaction (*lower curve*) and zein softening (*upper curve*), from Madeka and Kokini (1996). The number of proton populations detected by NMR is indicated at the bottom

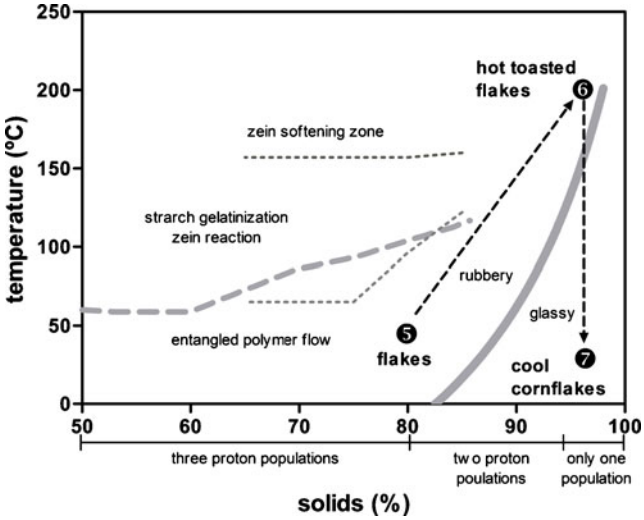

Fig. 7 State diagram for the final process stages of classical cornflake production: toasting and cooling. Solid line represents *Tg* curve for cornflakes, dashed line represents starch gelatinization onset temperature, and dotted line represents onset temperatures of zein crosslinking reaction (*lower curve*) and softening (*upper curve*), from Madeka and Kokini (1996). The number of proton populations detected by NMR is indicated at the bottom

The cornflake production process started with raw grits (point 1 on Fig. 6a) at ambient temperature, with a water content of 13 %, which was attained after the humidification step used in dry milling of kernels, with the purpose of facilitating the peeling of pericarp (Culbertson 2004). This water content was higher than the "hydration limit" water content determined by the GAB equation (9.1 %). Accordingly, the transversal relaxation time T_2 analyzed through the Hahn sequence showed the presence of two water populations, one of about 25 μs and the other of higher mobility with T_2 of 1.1 ms. At this stage, starch was in its native semicrystalline state, and DSC measurements confirmed that the amorphous regions of samples were in the glassy state. At these conditions, a low a_w (0.4) and a physical state that limit molecular mobility (crystalline and amorphous glassy regions) were combined to provide raw grit stability for several months according to producer specifications.

Before cooking, grits were mixed with water, salt, and sugar as formulation ingredients. During cooking in the aqueous formulation, water content increased and temperature reached 125 ºC (point 2 in Fig. 6a). The curved arrow indicates a possible path of temperature/composition changes. In the diagram of Fig. 6a, it can be clearly seen that during cooking, the samples were driven to the starch gelatinization zone over the T_{oG} curve determined by DSC which is also coincident with the reaction zone described by Madeka and Kokini (1996). The water content corresponded to the zone III where three proton populations were detected by NMR. At this stage, the high temperature and high molecular mobility promoted three main changes, starch gelatinization, zein crosslinking reaction, and the development of brown color and characteristic flavor of cereal food through Maillard reaction (Farroni and Buera 2012).

DSC thermograms of the samples after cooking revealed no starch gelatinization endotherms (Fig. 4), indicating that complete gelatinization occurred during the cooking stage. Also, when the samples were cooled up to −70 ºC immediately after cooking and then heated, frozen water was detected (Fig. 2). Thus, the water content and mobility at this stage allowed the melting of starch crystallites when heating and ice formation at subzero temperatures.

At the end of the cooking stage, the cooked grits had water content of 42.5 %. Then, their water content was reduced to about 21.6 % under hot-air current (120 ºC) (point 3 in Fig. 6a), which further promoted the development of the Maillard reaction, evidenced by the increase of brown color of dry cooked grits as compared to the ones leaving the cooking drum. The purpose of the drying step was to allow flaking without the material sticking in the rolls. At this drying temperature, the samples were still above of the T_{oG} curve and in zein reaction zone. Then, cooked grits were allowed to cool at an ambient temperature, remaining for 18 to 24 h in a bin in order to homogenize moisture distribution (point 4 on Fig. 6b). After this tempering stage, the grits were ready for flaking. It has to be noted that the remaining water content had to be high enough to maintain the samples in the rubbery state, with a soft texture necessary for flaking without ruptures. As the samples were located bellow the T_{oG} curve, starch underwent partial retrogradation during tempering (Fig. 4) which is known to facilitate the flaking process (Culbertson 2004). At these conditions, zeins are in the entangled polymer flow region which is located between the reaction temperature and glass transition (Madeka and Kokini 1996). In this way, the material is soft enough to be flaked without cracking. The friction of the corn material with the rolls during the flaking process increased the temperature, and some water was lost due to compression. After flaking, at 17.5 % humidity and 45 ºC (point 5 in Fig. 6b), the samples were still in the rubbery state and still soft.

In the toasting stage, the flaked grits were subjected to high temperature (close to 200 ºC) in an air-jet oven with good heat transfer (point 6 on Fig. 7). The water content at which FG entered the toasting oven (point 5 on Fig. 7) allowed a good development of the Maillard reaction, which was indicated by hydroxymethyl furfural content, and generated brown pigments and flavors typical of this product (Farroni and Buera 2012). In the toasting process, several rapid changes occurred; rapid water lost occurred while the increment of temperature maintained the sample in the rubbery zone. The final temperature reached is much higher than the T_g, and the crosslinked network developed in the previous steps became soft enough to be malleable. The sudden water evaporation distorted the matrix generating bubbles and resulting in a structure with macroscopic pores (Farroni and Buera 2012). The more

mobile water populations disappeared in this process, only the water highly interacting with solids remained. The final water content was lower than the hydration limit, m_o, determined by the GAB equation. When the cornflakes left the oven and cooled, as the water content was reduced, the cooled samples entered in the glassy zone (point 7 on Fig. 7). The samples underwent mechanical hardening, which allowed that bubbles were fixed in the rigid structure obtaining the typical blistered aspect and the crispy texture of breakfast cereals.

Conclusions

The dynamic approach of proton population analysis through their relaxation times allowed distinguishing of the different water sorption isotherm states on cornflakes based on an equilibrium thermodynamic approach. Since nonequilibrium states are being considered along the whole cornflake process stages, the limits of different zones traditionally defined for the water sorption stages can be better identified through the ^{1}H NMR T_2 relaxation times.

Thus, ^{1}H NMR studies represent an adequate way to define the mobility state of water and relate it to technological process and quality parameters in food.

GAB sorption isotherm modeling and DSC provided complementary information that was in accordance to NRM data.

The combination of techniques employed was useful to define the different water mobility states. NMR is a direct measure proton dynamics and, therefore, it was used as reference for zone delimitation of protons with different mobilities.

The development of characteristic cornflake appearance and flavor results from the occurrence of physical and chemical changes which determined the composition and microstructure of the final product. By describing the process using supplemented state diagrams, it was possible to delimitate regions in which the main components (starch and proteins) underwent specific changes such as gelatinization or crosslinking. The data of comparative mobility of water populations helped to understand the occurrence of those changes and the conditions prevailing in each stage.

The physical state of the sample could be explained for each process stage; the matrix was soft and malleable when important internal and external forces were applied, thus allowing the change of shape, microstructure, and appearance of the flaked product. Finally, physical hardening occurred after toasting and cooling to create the typical expected crispy texture.

Financial Support The present work was supported by the following research projects: UBACYT es 2011–2014, Universidad de Buenos Aires, and PICT 2008–0928 financed by Agencia Nacional de Promoción Científica y Tecnológica, Argentina.

References

AACC (1996). Approved methods of the American Association of Cereal Chemists. Method 44–16. AACC International, St. Paul, MN, USA.

Assifaoui, A., Champion, D., Chiotelli, E., & Verel, A. (2006). Characterization of water mobility in biscuit dough using a low-field ^{1}H NMR technique. *Carbohydrate Polymers, 64*, 197–204.

Buera, M. P., Roos, H., Levine, H., Slade, L., Corti, H. R., Reid, D. S., Auffret, T., & Angell, C. A. (2011a). State diagrams for improving processing and storage of foods, biological materials, and pharmaceuticals (IUPAC technical report). *Pure and Applied Chemistry, 83*(8), 1567–1617.

Buera P, Barbosa-Canovas G & Gutiérrez G (2011b) ISOPOW 11 Round table discussion and closing of ISOPOW practicum III, 9–10 September 2010. World of Food Science. Available at: http://www.worldfoodscience.org/cms/?pid=1005756. Accessed 5 March 2013.

Carr, H. Y., & Purcell, E. M. (1954). Effects of diffusion on free precession in nuclear magnetic resonance experiments. *Physical Review, 94*(3), 630–638.

Chen, C.-M., & Yeh, A.-I. (2001). Effect of amylose content on expansion of extruded rice pellet. *Cereal Chemistry Journal, 78*(3), 261–266.

Chen, P., Long, Z., Ruan, R., & Labuza, T. (1997). Nuclear magnetic resonance studies of water mobility in bread during storage. *Food Science and Technology, 30*, 178–183.

Chinachoti, P., Vittadini, E., Chatakanonda, P., & Vodovotz, Y. (2008). Characterization of molecular mobility in carbohydrate food systems by NMR. In G. A. Webb (Ed.), *Modern Magnetic Resonance* (pp. 1703–1712). Dordrecht, Netherlands: Springer.

Choi, S., & Kerr, W. (2003). ^{1}H NMR studies of molecular mobility in wheat starch. *Food Research International, 36*, 341–348.

Chung, H.-J., & Lim, S.-T. (2004). Physical aging of glassy normal and waxy rice starches: thermal and mechanical characterization. *Carbohydrate Polymers, 57*, 15–21.

Colquhoun, I., & Goodfellow, B. (1994). Nuclear magnetic resonance spectroscopy. In W. Reiginald (Ed.), *Spectroscopic techniques for food analysis* (pp. 87–145). New York, USA: VCH Publishers Inc.

Cova, A., Sandoval, A. J., Balsamo, V., & Müller, A. J. (2010). The effect of hydrophobic modifications on the adsorption isotherms of cassava starch. *Carbohydrate Polymers, 81*, 660–667.

Culbertson, J. D. (2004). Grain, cereal: ready to eat breakfast cereals. In S. J. Smith & Y. H. Hui (Eds.), *Food processing: principles and applications*. Oxford, UK: Blackwell.

Cuq, B., Abecassis, J., & Guilbert, S. (2003). State diagrams to help describe wheat bread processing. *International Journal of Food Science & Technology, 38*(7), 759–766.

Curti, E., Bubici, S., Carini, E., Baroni, S., & Vittadini, E. (2011). Water molecular dynamics during bread staling by nuclear magnetic resonance. *Food Science and Technology, 44*, 854–859.

Farhat, I. A., Mitchell, J. R., Blanshard, J. M. V., & Derbyshire, W. (1996). A pulsed ^{1}H NMR study of the hydration properties of extruded maize-sucrose mixtures. *Carbohydrate Polymers, 30*, 219–227.

Farroni, A. E., & Buera, M. P. (2012). Colour and surface fluorescence development and their relationship with Maillard reaction markers as influenced by structural changes during cornflakes production. *Food Chemistry, 135*, 1685–1691.

Farroni, A. E., Matiacevich, S. B., Guerrero, S., Alzamora, S., & Buera, M. P. (2008). Multi-level approach for the analysis of water effects in corn flakes. *Journal of Agricultural and Food Chemistry, 56*(15), 6447–6453.

Fast, R. B. (2000). Manufacturing technology of ready-to-eat cereals. In R. B. Fast & E. F. Caldwell (Eds.), *Breakfast cereals and how they are made* (pp. 17–54). St. Paul, Minnesota, U.S.A.: American Association of Cereal Chemist.

Fullerton, G. D., & Cameron, I. L. (1988). Relaxation of biological tissues. In F. W. Wehrli & J. B. Kneeland (Eds.), *Biomedical magnetic resonance imaging principles, methodology, and application* (pp. 115–155). New York, USA: VCH Publishers Inc.

Fundo, J. F., Fernandes, R., Almeida, P. M., Carvalho, A., Feio, G., Silva, C. L., & Quintas, M. A. (2014). Molecular mobility, composition and structure analysis in glycerol plasticised chitosan films. *Food Chemistry, 144*(1), 2–8.

Gabbott, P. (2008). A practical introduction to differential scanning calorimetry. In P. Gabbott (Ed.), *Principles and applications of thermal analysis* (pp. 1–50). Oxford, UK: Blackwell Publishing Ltd.

Gordon, M., & Taylor, J. S. (1952). Ideal copolymers and the 2nd order transitions of synthetic rubbers. 1. Non-crystalline copolymers. *Journal of Applied Chemistry, 2*(2), 493–500.

Greenspan, L. (1977). Humidity fixed points of binary saturated aqueous solutions. Journal of research of the National Bureau of Standards. Section A. *Physics and Chemistry, 81*, 89–95.

Gregg, S. J., & Sing, K. S. W. (1982). *Adsorption, surface area, and porosity*. UK: Academic Press London.

Hahn, E. L. (1950). Spin Echoes. *Physical Review, 80*(4), 580–594.

Katkov, I. I., & Levine, F. (2004). Prediction of the glass transition temperature of water solutions: comparison of different models. *Cryobiology, 49*(1), 62.

Levine, H., & Slade, L. (1989). Influences of the glassy and rubbery states on the thermal, mechanical, and structural properties of doughs and baked products. In H. Faridi & J. M. Faubion (Eds.), *Dough rheology and baked product texture* (pp. 157–330). New York, USA: Springer.

Levine, H., & Slade, L. (1992). Glass transitions in food. In H. Schwartzberg & H. Hartel (Eds.), *Physical chemistry of foods* (pp. 83–221). New York, USA: Marcel Dekker.

Levine, H., & Slade, L. (1991). *Water relationships in foods. Advances in the 1980s and trends for de 1990s*. New York, USA: Springer.

Lin, X., Ruan, R. R., Chen, P. L., Chung, M., Ye, X., Yang, T., Doona, C., & Wagner, T. (2006). NMR state diagram concept. *Journal of Food Science, 71*(9), R136–R145.

Liu, H., Yu, L., Chen, L., & Li, L. (2007). Retrogradation of corn starch after thermal treatment at different temperatures. *Carbohydrate Polymers, 69*, 756–762.

Lomauro, C. J., Bakshi, A. S., & Labuza, T. P. (1985). Evaluation of food moisture sorption isotherm equations part 1: Fruit, vegetable and meat products. *Food Science and Technology, 18*(2), 111–117.

Madeka, H., & Kokini, J. L. (1996). Effect of glass transition and cross-linking on rheological properties of zein: development of a preliminary state diagram. *Cereal Chemistry, 73*(4), 433–438.

Palou, E., Lopez-Malo, A., & Argaiz, A. (1997). Effect of temperature on the moisture sorption isotherms of some cookies and corn snacks. *Journal of Food Engineering, 31*(1), 85–93.

Rahman, M. S. (2006). State diagram of foods: its potential use in food processing and product stability. *Trends in Food Science & Technology, 17*, 129–141.

Roos, Y. H. (2003). Thermal analysis, state transitions and food quality. *Journal of Thermal Analysis and Calorimetry, 71*, 193–199.

Roos, Y. H., Karel, M., & Kokini, J. L. (1996). Glass transitions in low moisture and frozen foods: effects on shelf life and quality. *Food Technology, 50*(11), 95–108.

Ruan, R. R., & Chen, P. L. (1998). Nuclear magnetic resonance techniques. In *Water in foods and biological materials: a nuclear magnetic resonance approach* (pp. 17–24). Lancaster, Pennsylvania, USA: Technomic Publishing Co.

Sablani, S. S., Bruno, L., Kasapis, S., & Symaladevi, R. M. (2009). Thermal transitions of rice: development of a state diagram. *Journal of Food Engineering, 90*, 110–118.

Samapundo, S., Devlieghere, F., Meulenaer, B. D., Atukwase, A., Lamboni, Y., & Debevere, J. M. (2007). Sorption isotherms and isosteric heats of sorption of whole yellow dent corn. *Journal of Food Engineering, 79*(1), 168–175.

Sandoval, A. J., Nuñez, M., Müller, J. A., Della Valle, G., & Lourdin, D. (2009). Glass transition temperatures of a ready to eat breakfast cereal formulation and its main components determined by DSC and DMTA. *Carbohydrate Polymers, 76*, 528–534.

Schmidt, S. J. (2004). Water mobility in foods. *Advances in Food and Nutrition Research, 48*, 1–101.

Slade, L., & Levine, H. (1995). Glass transitions and water food structure interactions. *Advances in Food Nutrition Research, 38*, 103–269.

Slade, L., Levine, H., & Finley, J. W. (1989). Protein-water interactions: water as a plasticizer of gluten and other protein polymers. In R. D. Phillips & J. W. Finley (Eds.), *Protein quality and the effects of processing* (pp. 9–124). New York, USA: Marcel Dekker.

Tang, R. H., & Hills, B. B. (2001). A proton NMR relaxation study of the gelatinization and acid hydrolysis of native potato starch. *Carbohydrate Polymers, 46*, 7–18.

Thiewes, H., & Steeneken, P. (1997). The glass transition and the sub-*T*g endotherm of amorphous and native potato starch at low moisture content. *Carbohydrate Polymers, 32*, 123–130.

Timmermann, E. O., & Chirife, J. (1991). The physical state of water sorbed at high activities in starch in terms of the GAB sorption equation. *Journal of Food Engineering, 13*(17), 1–179.

Timmermann, E. O., Chirife, J., & Iglesias, H. A. (2001). Water sorption isotherms of foods and foodstuffs: BET or GAB parameters? *Journal of Food Engineering, 48*(1), 19–31.

Toufeili, I., Lambert, I. A., & Kokini, J. L. (2002). Effect of glass transition and cross-linking on rheological properties of gluten: development of a preliminary state diagram. *Cereal Chemistry, 79*(1), 138–142.

Wang, X., Choi, S. G., & Kerr, W. L. (2004). Water dynamics in white bread and starch gels as affected by water and gluten content. *Food Science and Technology, 37*, 377–384.

Yanniotis, S., & Blahovec, J. (2009). Model analysis of sorption isotherms. *Food Science and Technology, 42*, 1688–1695.